Sustainable Energy & Fuels

>10% solar-to-hydrogen efficiency unassisted water splitting on ALD-protected silicon heterojunction solar cells

Journal:	*Sustainable Energy & Fuels*
Manuscript ID	SE-ART-02-2019-000110.R1
Article Type:	Paper
Date Submitted by the Author:	29-Mar-2019
Complete List of Authors:	Tan, Chor Seng; Stanford University, Materials Science and Engineering Kemp, Kyle; Stanford University, Materials Science and Engineering Braun, Michael; Stanford University Meng, Andrew; Stanford University, Materials Science and Engineering Tan, Wanliang; Stanford University, Materials Science and Engineering Chidsey, C. E. D.; Stanford University, Chemistry Ma, Wen; Sunpreme Inc. Moghadam, Farhad; Sunpreme Inc. Mc Intyre, Paul; Stanford University, Department of Materials Science and Engineering

Title: >10% solar-to-hydrogen efficiency unassisted water splitting on ALD-protected silicon heterojunction solar cells*

Authors: Chor Seng Tan[†#], Kyle W. Kemp[†#], Michael Braun[†], Andrew C. Meng[†], Wanliang Tan[†], Chris E.D. Chidsey[‡], Wen Ma[§], Farhad Moghadam[§], and Paul C. McIntyre[†]

Abstract

Solar water splitting using photoelectrochemical cells (PEC's) is a promising pathway toward clean and sustainable storage of renewable energy. Practical realization of solar-driven synthesis of hydrogen and oxygen integrating light absorption and electrolysis of water has been challenging because of 1) the limited stability of good photovoltaic materials under the required electrochemical conditions, and 2) photovoltaic efficiency losses due to light absorption by catalysts, the electrolyte, and generated bubbles, or reflection at their various interfaces. Herein, we evaluate a novel integrated solar water splitting architecture using efficient silicon heterojunction photovoltaic cells that avoids such losses and exhibits a solar-to-hydrogen (STH) efficiency in excess of 10%. Series-connected silicon Heterojunction with Intrinsic Thin Layer (HIT) cells generate sufficient photovoltage for unassisted water splitting, with one of the cells acting as the photocathode. Platinum is deposited on the back (dark) junction of this HIT cell as the catalyst for the hydrogen evolution reaction (HER). The photocathode is protected from

* Electronic supplementary information (ESI) available.

† Department of Materials Science and Engineering, Stanford University, Stanford, CA, USA
‡ Department of Chemistry, Stanford University, Stanford, CA, USA
§ Sunpreme Inc., Sunnyvale, CA, USA
# Both authors contributed equally to this work

corrosion by a TiO_2 layer deposited by atomic layer deposition (ALD) interposed between the HIT cell and the Pt, enabling stable operation for > 120 hours. Combined with oxygen evolution reaction (OER) catalysts deposited on a porous metal dark anode, these PEC's achieve stable water splitting with a record high STH efficiency for an integrated silicon photosynthesis device.

Introduction

The past decade has seen growing adoption of clean and renewable energy sources such as wind and solar as an alternative to fossils fuels for generation of electric power. Solar power has drawn great interest due to its abundance – approximately 120,000 TW of solar energy is, in principle, accessible globally[1], dwarfing humanity's global power consumption. Photovoltaic cells can capture a portion of this vast energy source and convert it to electricity, with a long-term trend of increasing efficiency and decreasing cost[2]. However, the intermittent nature of sunlight is an obstacle to large-scale grid implementation of solar energy, as it will eventually require some form of energy storage to act as a reservoir to allow constant and on-demand delivery of power.

One possible solution to this problem is solar-driven electrolysis of water, which collects and stores solar energy in the form of the chemical bonds in molecular fuels, such as hydrogen. Hydrogen is storable and transportable, and can either be combusted or recombined with oxygen in a fuel cell to generate electricity when it is needed. Hydrogen can also be used as feedstock for ammonia fertilizer production, essential to global food supply, and the protons and electrons produced by water oxidation are required ingredients for electrochemical synthesis of liquid fuels by CO_2 reduction[3].

There are two major paradigms for water splitting systems: 1) an integrated photoelectrochemical cell (PEC) in which a photoabsorber is electrically coupled to efficient catalysts for water oxidation and/or hydrogen evolution; and 2) separate photovoltaic and

electrochemical cells ("PV + electrolyzer") which are wired together. There is considerable debate about the relative merits of these two approaches. Analysis of the costs of solar-to-hydrogen systems have provided estimates ranging from ~ \$3-10 kg^{-1} for integrated PEC's [4,5] and ~\$5-8 kg^{-1} for PV + electrolyzer systems[6,7]. These projected costs are similar and the ranges are overlapping. PV + electrolyzer systems have the practical advantage of utilizing off-the-shelf technologies such as commercial silicon solar cells and polymer electrolyte membrane (PEM) electrolyzers. However, PEM electrolyzers operate at large current densities (1-2 A/cm^2) and use large loadings of expensive noble metal catalysts[8]. Advantages of PEC's are 1) the potential simplicity of an integrated design, 2) their compact foot-print in which a similar projected device area can be used for light absorption and electrochemistry, and 3) their ability to accommodate a wide range of catalysts because they operate at electrolysis current densities better matched to solar photocurrent densities.

PEC cells have been widely studied since 1972, when Fujishima and Honda reported the first demonstration of photoelectrochemical water splitting using a single crystal TiO_2 photoanode and a Pt cathode[9]. Since then, there have been significant technical advances in PEC cell technology. Due to the relatively high voltage (typically $\geq$ 1.8 V) that is required to drive the overall water splitting reaction, coupled with the requirements for stability in contact with aqueous solutions for the conduction and valence bands of the semiconductor to straddle the potentials for proton reduction and water oxidation, only materials with wide band gaps, such as TiO_2, WO_3, $SrTiO_3$, and SiC are capable of unassisted water splitting in a single junction device[10,11,12]. However, the band gap requirement means that such devices have low STH efficiencies as they can only absorb a small portion of the solar spectrum. To overcome this

efficiency problem, solar-powered PEC water splitting devices can employ a multijunction architecture with two or three cells connected in series in order to provide the necessary operating voltage[13,14,15].

For such a technology to be commercially viable, devices for water splitting must be efficient, stable, and have a path to low cost at large scale. Most of the top-performing devices for unassisted water splitting reported thus far, however, utilize expensive III-V materials such as InGaP and GaAs, which are unlikely to be economical without significant solar concentration[15,16,17]. These absorber materials, along with others such as the perovskites, are also generally unstable under oxidizing potentials and, in some cases, under reducing potentials[14] and are unlikely to be used for large scale applications in the near-term future[18,19].

In order to be commercially viable, inexpensive materials such as silicon have to be used as the photoabsorber material. Other groups have previously investigated using tandem and triple-junction a-Si solar cells as photocathodes for water splitting, achieving as high as 2.93%[20] and 7.8%[21,22,23,24] STH efficiency conversion respectively. However, the stability of the photocathodes were mostly limited to a few hours in the concentrated acid and base electrolytes investigated. Reece et al. used a triple junction a-Si cell as a photoanode in 1 M potassium borate buffer, achieving a 4.7% STH efficiency and 3 hours of stable operation[25]. Urbain et al. reported a STH efficiency of 9.5% using a monolithic a-Si:H/a-Si:H/lc-Si:H/lc-Si:H quadruple junction solar cell as the photocathode in 1 M KOH, however it was stable for less than 1000 s[26]. More recently, groups have studied using silicon heterojunction solar cells to achieve greater STH efficiencies. Silicon Heterojunction with Intrinsic Thin layer (HIT) solar cells have demonstrated

high open circuit voltages of over 740 mV, short circuit current densities over 40 $mAcm^{-2}$, and photovoltaic efficiencies as high as 25.6% due to the excellent passivation of the c-Si by ultrathin intrinsic a-Si layers, making them an excellent candidate for water splitting with superior performance over the likes of a-Si solar cells[27, 28]. Song et al.[29] demonstrated 9.54% STH efficiency in 1 M NaOH using four such cells connected in series, while Schuttaff et al.[30] achieved 14.2% using three cells in series in 1 M KOH. While they reported operating stabilities of 25 h and 100 h respectively, this was achieved using a "PV+electrolyzer" configuration, where the silicon solar cells are not in contact in the electrolyte. This results in a bulkier and potentially more expensive device. In the latter case[30], the active area for electrolysis was over 10 times greater than that of the silicon cells.

We present an efficient, integrated solar water splitting device using silicon HIT cells. A corrosion-resistant ALD TiO_2 protection layer imparts chemical stability while electrically coupling the HIT cell to an efficient HER catalysts, enabling the HIT cells to operate in contact with either highly-corrosive electrolytes such as 1 M H_2SO_4 or with pH 7 buffer solution without any loss of photovoltaic performance. This negates a common disadvantage of the integrated design over a PV + electrolyzer configuration - the poor stability of the absorber material under electrochemical reaction conditions. In the reported device design, light absorption and catalytic activity occur on different sides of the device, circumventing the parasitic losses caused by light scattering/absorption by the catalysts, electrolyte, protection layers, and generated bubbles [30,31], problems commonly suffered by other reported integrated devices[32]. The cell design also avoids any possible instability of silicon under anodic potentials. By connecting three silicon HIT solar cells in series, using an atomic layer deposited (ALD) TiO_2 protection layer, and contacting the

silicon photocathode with a porous metal dark anode across a thin electrochemical flow cell, unassisted water splitting with > 10% solar-to-hydrogen efficiency under one sun illumination is demonstrated. This is, to our knowledge, the highest reported efficiency for integrated devices using silicon absorbers only, exceeding that of other reports of water splitting devices using tandem or triple-junction amorphous silicon heterojunction solar cells arranged in series [21,22, 24, 25, 26, 33] . The protected HIT cell photocathode was chemically unchanged after 120 hours of operation in concentrated acid, and suffered no loss in water splitting efficiency, showing it is possible to match, or even exceed, both the efficiency and stability of PV+electrolyzer configurations [29,30,34,35] with a much more compact, integrated design.

Experimental

Preparation of silicon HIT cell

Bifacial silicon HIT cells were obtained from Sunpreme[**], which use thin amorphous silicon films to produce a p-i-(Si substrate)-i-n junction. Each of the four amorphous Si films is ultra-thin at about 10 nm thick. The cell current is collected by blanket layers of transparent indium tin oxide on both faces, with metallized copper grids deposited on top to enhance electrical conduction. More details about the cells are included in S18 of the supplementary information. For the purposes of testing, 6-inch by 6-inch Si HIT cells are laser cut into 1.5 cm x 1.5 cm pieces.

The HIT cells are cleaned using a Diener Pico oxygen plasma cleaner for 2 minutes to remove the impurities and contaminants on the surface. ALD TiO_2 is deposited on the ITO coating on the n-type back side of the HIT cells by atomic layer deposition (ALD) in a custom-built load-locked ALD reactor, using tetrakisdimethylamido-titanium (TDMAT) and H_2O as the titanium and oxygen precursors respectively at a substrate temperature of either 45° C or 150° C. The TDMAT bubbler temperature is kept at 80° C and the ALD chamber base pressure is about 1.0e-6 Torr. The TiO_2 film thickness and growth rate are determined by ellipsometry on a Si (100) test wafer that is placed in the ALD reactor alongside the HIT cell during deposition, and also confirmed with x-ray reflectivity (XRR) and cross-section transmission electron microscope (TEM) imaging.

[**] http://sunpreme.com/symmetric-bifacial-architecture/

Metallization is done in a Kurt J. Lesker sputtering system. The sides of the HIT cells are masked by Kapton tape to avoid depositing along the cell sides which might cause shorting. Titanium and Pt films of 50 nm thickness are deposited via DC sputtering in an argon atmosphere with a pressure of 50 mTorr and a flow rate of 3 sccm. The deposition is done at a rate of 5 nm/min and 10 nm/min for Ti and Pt, respectively, at a sputtering power of 200W and substrate temperature of 20° C.

OER catalyst

Porous Ti sheet substrates are sawcut and then rounded on a lathe with a carbide lathe bit to make them into circles with 1.3 cm diameter. Before depositing the OER catalyst, they are cleaned by sonicating in acetone/IPA/DI water for 20 minutes each. IrO_x OER catalyst, for device testing across a full range of solution pH, is deposited on the porous Ti substrate by dip-coating in 0.01 M iridium acetylacetonate dissolved in chloroform, and then calcined in air at 320°C for 1 hour in a tube furnace to decompose and remove the acetylacetonate ligands and oxidize the Ir to IrO_x[36,37] .

Solid state photovoltaic characterization

For solid state I-V testing, a 450 W Oriel Sol3A Class AAA Solar Simulator with an AM 1.5 filter was used. The intensity was calibrated to 100 $mWcm^{-2}$ by a standard Si reference diode.

The current-voltage measurements were made using a Keithley 2420 Source meter. The HIT cells were illuminated from the unmodified p-type top side with a 1 cm^2 aperture.

For chronoamperometry testing, we used a 300 W SF-300-A small collimated beam Class AAA solar simulator from ScienceTech.

Electrochemistry and PEC testing

Electrochemical characterization was carried out using a Biologic VSP potentiostat running EC-Lab on a PC. For 3-electrode experiments, a Ag/AgCl electrode in saturated KCl and a Pt wire were used as the reference and counter electrodes respectively. The stability of the ALD protected Si HIT cell is measured in a three-electrode set up. The HIT cell is epoxied, with DP 460 NS epoxy from 3M, to a strip of copper tape on a microscope glass slide, with a 1 cm^2 aperture cut in it for illumination. Testing is done in a 10 mm path length SR-101A visible range borosilicate glass spectrophotometer cell from Spectrocell Inc., with the unaltered top of the HIT cell exposed to illumination and the back side with the TiO_2/Ti/Pt stack in contact with the electrolyte. OER catalyst testing is also conducted in a three-electrode set up in a Teflon cone cell that is pressure sealed as previously reported in our group[38]. For triple-cell testing, a 2-electrode set up was used with the OER catalyst and the ALD protected HIT cell as the working and counter electrodes respectively. All the HIT cells had 0.95 cm^2 round metal apertures (for a total area of 2.85 cm^2) to define the active area of the device. A peristaltic pump was used to circulate the electrolyte in the flow cell. Linear sweep voltammetry is performed at a 10 mVs^{-1} sweep rate.

Materials Characterization

X-ray reflectivity was conducted using a PANalytical X'Pert PRO x-ray diffraction system. Scanning electron microscope (SEM) images were collected using a FEI Helios NanoLab 600i DualBeam Focused Ion Beam/Scanning Electron Microscope with 2 kV acceleration voltage and 43 pA beam current. A PHI 700 Scanning Auger Nanoprobe was used for Auger mapping of elemental surface compositions of the IrO_x OER catalysts on porous Ti sheet anodes. Transmission electron microscope (TEM) imaging and energy dispersive x-ray spectroscopy (EDS) was performed using a FEI Titan ETEM at an accelerating voltage of 300 kV.

Results

ALD protected Silicon HIT cell performance and stability – The silicon HIT photovoltaic cells on 6" wafers used in these experiments exhibit high fill factors of 0.80 to 0.82, V_{oc} of 740 – 750 mV and an efficiency of over 23%[39]. For assembly of multi-junction PEC's, these wafers were laser cut into 1.5 cm x 1.5 cm cells. The damage from the laser cutting, edge recombination effects of the smaller cells, absence of the copper bus bars (because they block a significant portion of incident light for the smaller cells), and some shadowing from the metal masks used during these measurements cause PV performance degradation, resulting in a diminished fill factor of about 0.70, a V_{oc} of 670 mV and a photovoltaic efficiency of about 18.0%. Employing full wafers rather than small test coupons used in our electrochemical measurements would recover the higher photovoltaic performance specified for these solar cells significantly, and thus boost the solar-to-hydrogen efficiency over the values reported here-in.

HIT cells fabricated either with or without metallized copper grids on the back (n^+) amorphous silicon (a-Si) junction were investigated. Cells without metallized grids were used as the photocathode for the electrochemical reaction. To protect the photocathodes from corrosion during water splitting, TiO_2 was deposited on the ITO coating by ALD. Subsequently, the TiO_2-coated back side of the HIT cell was metallized by sputter deposition of 50 nm of Ti followed by 50 nm of Pt (see schematic in figure 1(a)). Figure S1 in the supplementary show TEM cross-section images of such a device, while S2 shows some EDS line scans of the different layers in the device.

Titanium produces a favorable band alignment to the conduction bands of TiO_2 and a-Si and also acts as a adhesion layer to improve the adhesion of metal catalysts[40]. Because of the good band alignment between the conduction bands of the TiO_2 and the n-doped amorphous silicon, addition of the TiO_2 protection layer enhances the stability of the HIT cell without causing any significant degradation in the HIT cell performance. Electrons are transported across the TiO_2 without encountering a significant energy barrier[41,42], as illustrated in figure 1(b). This lack of TiO_2-thickness dependence of the series resistance of the HIT cells allows use of relatively thick TiO_2 protection layers without suffering a loss in performance.

However, as the TDMAT/H_2O ALD process is typically carried out at a temperature of 150° C or higher, some degradation in solid state performance of the silicon HIT cells occurs during the process, possibly due to dehydrogenation of the amorphous silicon and poorer passivation of the c-Si device [43,44]. As shown in figure 2(a), there is a decrease in the V_{oc} of the HIT cell of 30 mV. Moreover, an increase in series resistance in the HIT cells results in the fill factor dropping from greater than 70% to approximately 65% for cells with ALD TiO_2 relative to those without TiO_2. The photovoltaic efficiency decreases to ~15% as a result, for both 7.0 nm and 35 nm thick TiO_2 films. This degradation is clearly related to the process temperature as it is observed even when the Si HIT cell is held at the usual ALD temperature without performing any deposition (see figure S3 of the supplementary information).

This performance degradation can be avoided when the ALD TiO_2 deposition is carried out at a lower substrate temperature of 45° C, which results in a slightly higher growth rate of about 0.9 Å/cycle. The thickness and growth per cycle were verified using XRR (S4 in supplementary

information). This increase in ALD-TiO_2 growth per cycle at lower deposition temperatures has also been observed by other groups[45]. As shown in Fig. 2(a), when the ALD is carried out at this lower temperature, the overall photovoltaic performance of the HIT cell remains undiminished even after the deposition of 9 nm of TiO_2 layers. As with the samples on which TiO_2 was deposited at 150° C, the thickness of the TiO_2 layer has little effect on the I-V characteristics of the HIT cells (see S5).

To further verify that the ALD TiO_2 layer does not cause any increase in the series resistance, we deposited TiO_2 of different thickness in the range of 2 to 15 nm on n^+Si, which has a similar conduction band edge energy as amorphous Si[46], followed by metallization with 50 nm of Ti and Pt on top as in the HIT cells, along with 100 nm of Al on the back side to form an ohmic contact. We observed that the sample resistance does not change detectably with TiO_2 thickness during cyclic voltammetry in 10 mM ferri/ferrocyanide standard redox couple (figure S6 in the supplementary information).

To study the effect of the TiO_2 protection layer on the stability of the HIT cell during HER, TiO_2-protected and unprotected samples were bonded by epoxy to copper tape on a glass slide and tested in a 3-electrode configuration in a cuvette cell in 1 M H_2SO_4(aq) solution under simulated 1 sun illumination. Cyclic voltammetry sweeps in figure 2(b) show an onset voltage for hydrogen evolution exceeding 600 mV under illumination, and a photovoltage of 670 mV when compared with a n^+Si sample measured in the dark, which matches the measured V_{oc} from solid state photovoltaic I-V measurements. The saturated current density exceeded 38 $mAcm^{-2}$. Because light absorption and HER occur on different sides of the photocathode, optical losses

due to light attenuation through the catalyst layers is not an issue. The TiO_2-protected silicon HIT photocathode showed similarly high photovoltages in neutral pH phosphate buffer and in 1 M NaOH electrolytes, showing that it can be applied to a wide range of pH electrolytes (see figure S7).

In order to study the stability of the ALD TiO_2-protected HIT cells, chronoamperometry was conducted with the applied potential held at 0.2 V vs. RHE, such that the current densities were above 30 $mAcm^{-2}$, a desirable condition at which to operate the triple cell for unassisted water splitting. Without a TiO_2 protection layer, the HIT cell degraded within minutes in 1 M H_2SO_4, as shown by the decrease in current density during chronoamperometry in figure 3(a). The main degradation mechanism observed was rapid etching of the ITO coating on the HIT cell in the strong acid electrolyte, which caused delamination of the overlying layers from the silicon. This coincided with an abrupt drop in current density due to loss of electrical contact to (and physical loss of) the Pt HER catalyst. This is confirmed by XPS and Auger mapping of a sample tested area after failure, which detects only silicon on the surface (see S8). The addition of a TiO_2 protection layer greatly enhanced cell stability. The presence of 9 nm of TiO_2 deposited at 45° C allowed the HIT cell to operate at a stable current density for 4 hours; however, a 56 nm thick TiO_2 layer could operate stably for over 24 hours. A cyclic voltammetry scan in figure 3(b) after 24 hours of chronoamperometry testing shows no performance degradation.

Meanwhile, TiO_2 films deposited at 150° C were found to impart much better stability than films of similar thicknesses deposited at 45° C. A 7 nm thick film deposited at 150° C exhibited the same > 24 hours of stability (as shown in figure 3(c)) as the 56 nm thick film deposited at lower

temperature. This is possibly due to the higher density of the film deposited at higher temperature (see S4 of the supplementary information).

IrO_x on porous Ti OER catalyst - In order to achieve the highest possible STH efficiency in the water splitting cell, a low OER catalyst overpotential < 300 mV is essential. We used 3D porous Ti substrates with 1 mm thickness and 50 um pore sizes (figure 4(a)) to increase the contact area between the electrolyte and the catalyst, thus increasing the geometrical density of active sites for OER. We employed Auger mapping (figure 4(b)) to show uniform coverage of Ir over the Ti substrate. The dip-coated IrO_x on a porous Ti substrate achieved an overpotential of 250 mV at 10 $mAcm^{-2}$ in 1 M H_2SO_4. This OER catalyst is of interest because it can be used to test PEC performance across a full range of solution pH due to its excellent stability. IrO_x on porous Ti tested in 1 M NaOH exhibited a higher overpotential of 300 mV at 10 $mAcm^{-2}$, consistent with the reported reduction of catalytic activity of IrO_x in base[47]. Chronoamperometry was performed in acid to study the stability of the OER catalyst under operation (figure 4(d)), and a gradual current decay was observed, which is in agreement with other reports[36,48]. The decay has been attributed to diminished activity as the surface of the Ir is increasingly oxidized at anodic potentials sufficient to split water[48]. Others have also found evidence of the formation of a soluble Ir species of a higher oxidation state at anodic potentials and its subsequent removal due to dissolution[48,49]. However, the original activity could be recovered by a potential sweep to less positive potentials[48]. Our results agree with this proposal, as cyclic voltammetry scans after chronoamperometry showed no degradation in performance.

Triple cell STH efficiency and stability – To perform unassisted water splitting, three silicon HIT cells were mounted side by side on a titanium plate, each with a 0.95 cm^2 aperture mask that controls the illumination area. The photocathode was connected with the electrolyte in a Teflon flow cell, through which the electrolyte flowed through two inlets and two outlets, and was sealed by mechanical pressure. Two additional HIT cells with metal grids on both sides were used to provide the additional external photovoltage (solid state data in S9) to drive the water splitting reaction. The external HIT cells were electrically connected to a titanium anode housing which holds the porous OER electrocatalyst on the opposite side of the flow cell. A schematic of the complete flow cell is shown in figure 5(a) with additional photographs in S10 of the supplementary information.

Current-voltage measurements were performed on these cells by providing a potential between the silicon HIT cells and the electroanode on both sides of the flow cell. In the absence of competing redox couples, the Faradaic efficiency of the H_2 and O_2 evolution processes approach 100%[50,51]. The STH efficiency of a water splitting cell is calculated according to Eq.1:

$$STH\% = \frac{(I_{ph}(mAcm^{-2})(1.23\ V))}{P(mWcm^{-2})} \quad (1)$$

Where P is the output power of the solar simulator (100 $mWcm^{-2}$ to simulate 1 sun intensity), and I_{ph} is the photocurrent at 0 V bias. Three series-connected HIT cells, one acting as the photocathode, and an IrO_x OER catalyst-coated porous Ti exhibited an STH efficiency of 12.2%

in concentrated acid (figure 5(b)). If we account for losses due to solution resistance (as explained in S11 of the supplementary information), the STH efficiency increases to 14.5%.

Chronoamperometry was conducted at a constant applied potential of 1.23 V with just a single TiO_2-protected HIT cell in contact with the flow cell in 1 M H_2SO_4. We performed two successive chronoamperometry measurements for 3 and 9 hours respectively for a HIT cell with TiO_2 deposited at 45° C, with cyclic voltammetry scans performed in between as shown in figure 5(c), and observed no deterioration in the performance as seen from the cyclic voltammetry scans afterwards, proving that the HIT cell was still well protected by the ALD TiO_2 layer after a total of 12 hours of operation in the flow cell. With a 35 nm TiO_2 film deposited at 150° C, no deterioration in the cyclic voltammetry was observed even after 120 hours of chronoamperometry testing, confirming the superior protection afforded at HER potentials by the TiO_2 deposited at the higher temperature. XPS and Auger mapping of this sample after 120 hours of testing showed no chemical change to the surface (see S12). Although the sample that showed 120 hours of stability had poorer CV performance than the 45°C – deposited TiO_2 HIT cell, the best performing HIT cell with TiO_2 deposited under the same conditions had performance similar to the 45° C – deposited TiO_2 HIT cell (see S13). Therefore, >10% STH efficiency can also be achieved when the ALD-TiO_2 protection layer is deposited at the higher temperature.

Discussion

The US Department of Energy has published a 2020 cost target of $2.30/kg for the production of hydrogen from water electrolysis, including photoelectrochemical methods, with the ultimate goal being $2.00/kg[52]. Recent analysis suggests that a STH efficiency of 10% is the breakeven point for energy return on investment[53]. These experiments demonstrate that the efficiency target is possible using silicon solar cells in a compact, integrated configuration compared to a side-by-side configuration of photoanode and photocathode, with stability exceeding 120 hours. Table 1 summarizes the reported efficiencies and stability information for silicon-based water splitting devices using both the integrated (PEC-anode or PEC cathode) and the PV + electrolyzer configurations. All the devices were measured in a two-electrode setup under 1 sun illumination. Comparing the results obtained in this study, none of the previously reported devices managed to achieve a similar combination of high efficiency and stability within a compact device architecture. Only the PV + electrolyzer configuration has been able to achieve a 10% STH efficiency target, of which only one has managed a higher efficiency than is reported herein, albeit by using an electrolyzer with 10x larger surface area than the photoabsorber. All other integrated devices had STH efficiencies less than 10%.

With optimization of the OER catalyst to further lower the overpotential, and use of large area silicon HIT cells to recover their full open circuit voltage and fill factors, a pathway exists to achieve an STH efficiency in excess of 15%. Currently the flow cell only has roughly the geometric area of a single Si HIT cell, we can further enhance the water splitting efficiency by extending the flow cell below the external Si HIT cells and increasing the surface area of the

catalysts. This should further lower the overpotentials and also provide cooling for the external cells that will mitigate the heat-induced performance degradation (approximately -0.25%/C[54,55]). We also believe that far greater stability is possible. The main mode of failure in our experiments in 1 M H_2SO_4 is under-cutting of the catalyst, contact and protection layers by selective etching of the underlying ITO layer. Pinholes in the catalyst, metallic contact and protective films, possibly due to the roughness of the ITO layer on the HIT cell back side and to dust particles and contamination on the ITO surface after completion of solar cell fabrication and sample handling lead to eventual device failure. Coating of the wafer back side with the ALD-TiO_2 protection layer and the sputtered metal contact and HER catalyst layers used in this work did not take place in a cleanroom. Therefore, dust particles are inevitable, and these can easily settle in the grooves of the highly-textured HIT cell surface (see S14 of the supplementary information), causing incomplete film coverage. The superior stability displayed by the TiO_2 deposited at 150°C may be due to the higher density and better conformality of deposition over the rough ITO back-side contact of the HIT cells at this temperature, which lies within the window of true, surface-saturating ALD for TDMAT/H_2O chemistry[56]. The chemical stability of the TiO_2 film is also likely to be greater for higher deposition temperatures[57]. Eliminating the ITO layer in the as-received HIT cells, which is unnecessary in our design as we illuminate the cells from the front side, would be a simple route to improved endurance. An ALD-TiO_2/Ti/Pt stack with 10 nm of TiO_2 deposited at 45° C on a polished n^+Si substrate (no ITO layer) showed no degradation in performance after 120 hours of continuous operation in acid (figure S15).

These experiments use Pt and IrO_x catalysts for ease of demonstration as they are widely accepted as benchmark electrocatalysts for HER and OER, respectively. However, their scarcity

prompts interest in alternative catalyst materials. It should be noted that our multi-junction HIT photoelectrochemical cell design can flexibly accommodate many different choices for HER and OER catalysts. For example, the Pt HER catalyst could be replaced by more inexpensive options that use more Earth-abundant materials, such as MoS_2[58]. Possible replacements for IrO_x as the OER catalyst in acid are limited due to stability concerns; however, these cells also operate efficiently in basic as well as neutral pH electrolyte (see figure S16), where alternative OER catalysts based on non-precious metals such as Ni, Fe, and Co have been shown to out-perform IrO_x while exhibiting excellent stability[59,60, 35]. Operating the flow cell in neutral pH electrolytes is of particular interest due to safety concerns with extreme pH electrolytes. Despite higher HER and OER overpotentials and greater resistive losses in neutral phosphate buffer solution, by adding an extra Si HIT cell, it is possible to achieve over 10% STH efficiency (see S17). These results indicate the possibility of substituting more abundant alternatives for platinum and iridium metal catalysts without compromising the STH efficiency.

Conclusion

In summary, we demonstrate unassisted photoelectrochemical water splitting driven by the photovoltage of series-connected silicon HIT cells, in which ALD-grown TiO_2 protection layers inhibit corrosion during the hydrogen evolution reaction and electronically couple the silicon photocathode to an efficient HER catalyst. Using IrO_x on porous Ti as the OER catalyst, greater than 10% STH efficiency was achieved in both 1 M H_2SO_4 and 1 M NaOH electrolyte. The device design, in which the illumination occurs on the side of the solar cell opposite the electrochemical reaction, avoids both parasitic losses due to light absorption and reflection and any instability of silicon at anodic potentials. We have shown that it is possible to achieve high conversion efficiencies with good device stability by using a compact, all-silicon light absorber design in which integration with an electrochemical flow cell does not inherently reduce photovoltaic efficiency.

Conflicts of Interest

There are no conflicts to declare.

Acknowledgements

This work was supported by National Science Foundation award CBET-1336844 and by the Stanford Energy 3.0 industrial affiliates program. We also thank Farhad Moghadam and Wen Ma of Sunpreme Inc. for generously providing us with the silicon HIT cells. Part of this work was performed at the Stanford Nano Shared Facilities (SNSF), supported by the National Science Foundation under award ECCS-1542152. Author C.S.T. also received funding support from the Agency for Science, Technology and Research (A*STAR) for his Ph.D program.

Author Contributions

P.C.M and C.E.D.C directed the research. K.W.K and P.C.M conceived the idea. C.S.T and K.W.K designed and performed the experiments. M.B, A.C.M and W.T helped with materials characterization. C.S.T, K.W.K and P.C.M participated in the writing of the manuscript.

Figure 1

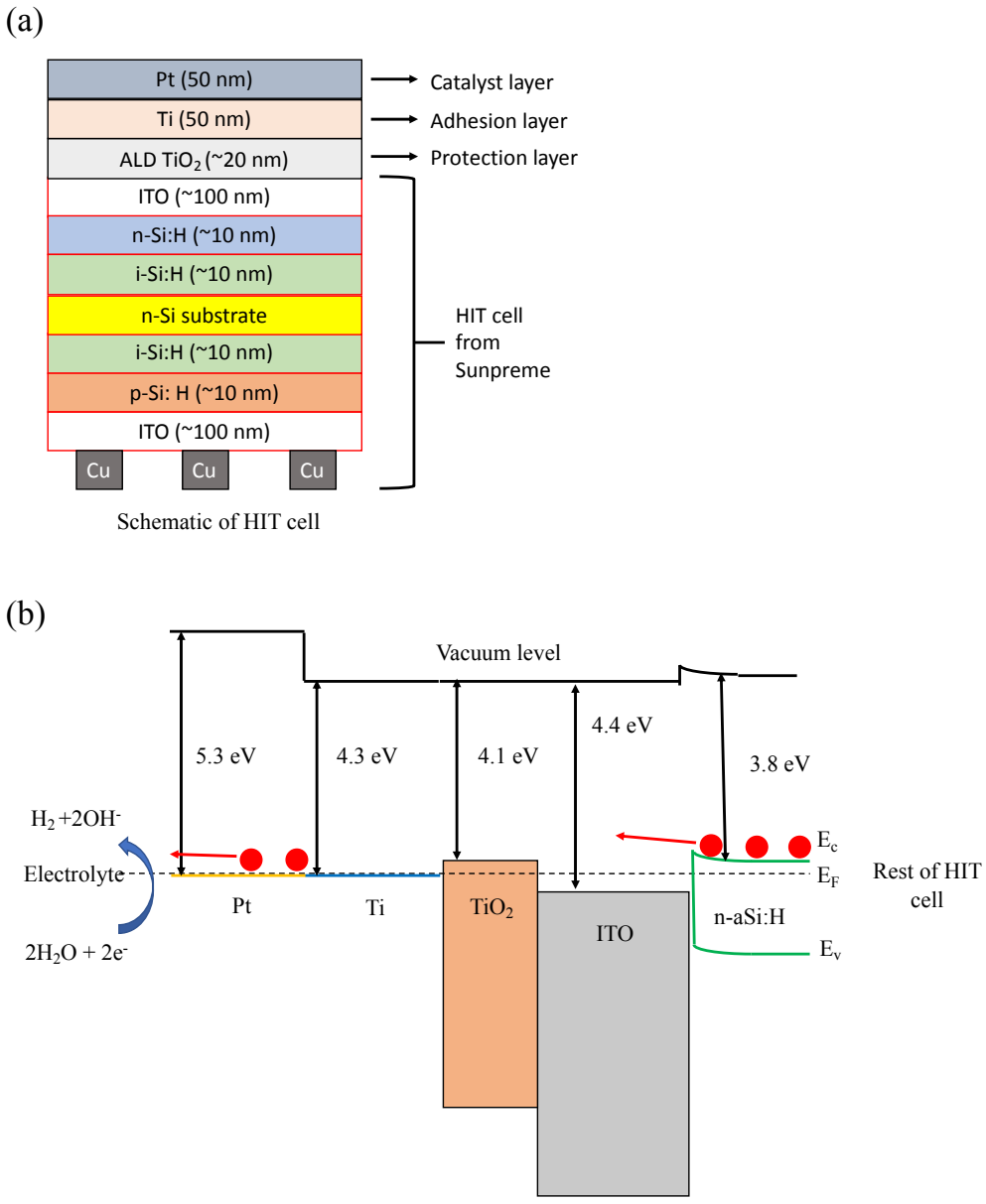

Fig. 1(a) – Schematic of silicon HIT cell with ALD TiO_2 protection layer and sputter deposited Ti/Pt metal stack; (b) band diagram of Si HIT cell/ITO/TiO_2/Ti/Pt shows a band alignment that facilitates the transfer of photogenerated electrons from the Si HIT cell through the ALD TiO_2 layer to the Pt/electrolyte interface. We assume reported[42,61,62] work functions and electron affinities for the various materials depicted in the stack, without interface dipoles that might shift band offsets.

Figure 2

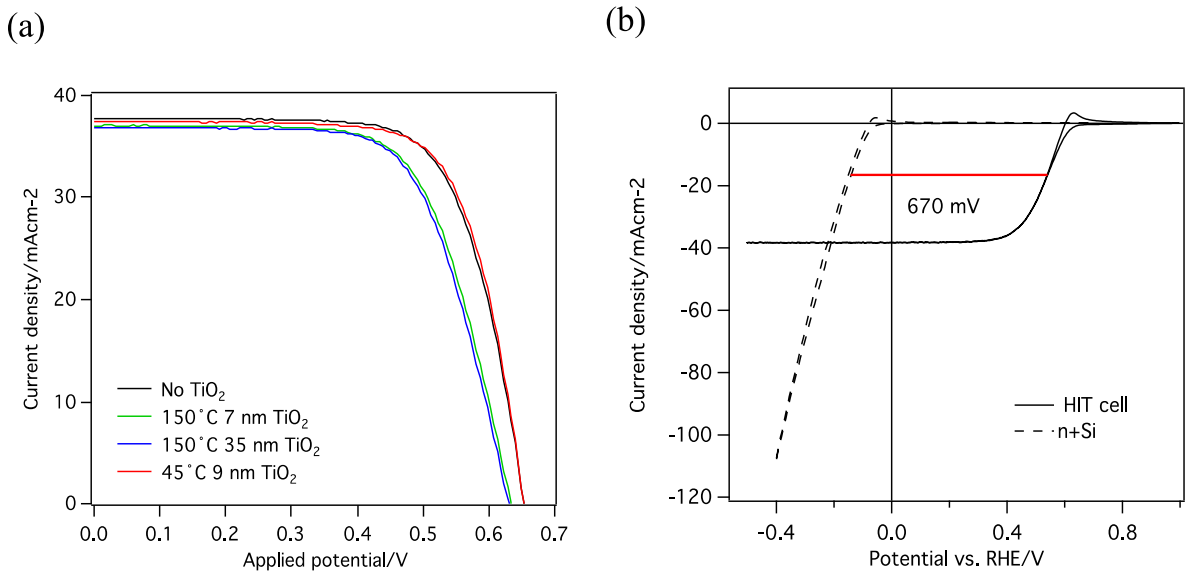

Fig. 2(a) – Solid state I-V data for an as-received HIT cell (black) and HIT cells with a 7 nm (green) and 35 nm (blue) ALD TiO_2 layer deposited at 150° C, and one with a 9 nm (red) TiO_2 layer deposited at 45°C with 50 nm Ti/50 nm Pt metal coating deposited by sputter deposition; (b) cyclic voltammetry of a HIT cell and a n^+Si sample (tested in the dark) protected by TiO_2 deposited at 45°C in 1 M H_2SO_4. A potential shift of 670 mV is measured between the two scans, representing the photovoltage generated by the HIT cell.

Figure 3

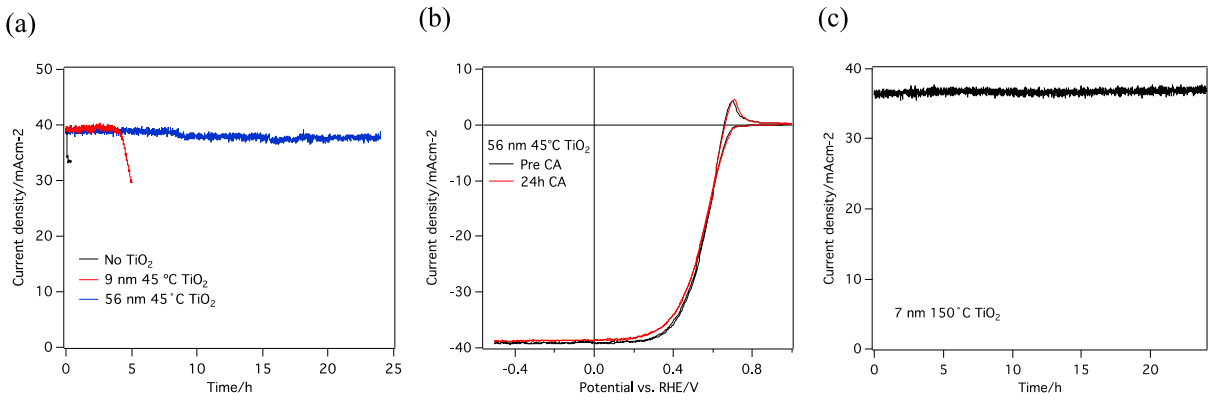

Fig. 3(a) Chronoamperometry at 0.2 V vs. RHE of HIT cell with no TiO_2, 9 nm TiO_2 and 56 nm TiO_2 (black, red and blue curves respectively) deposited at 45 °C in 1 M H_2SO_4 ; (b) cyclic voltammetry showing no degradation in device performance after 24 hours of continuous operation; (c) chronoamperometry at 0.2 V vs. RHE of a HIT cell with 7 nm TiO_2 deposited at 150°C in 1 M H_2SO_4.

Figure 4

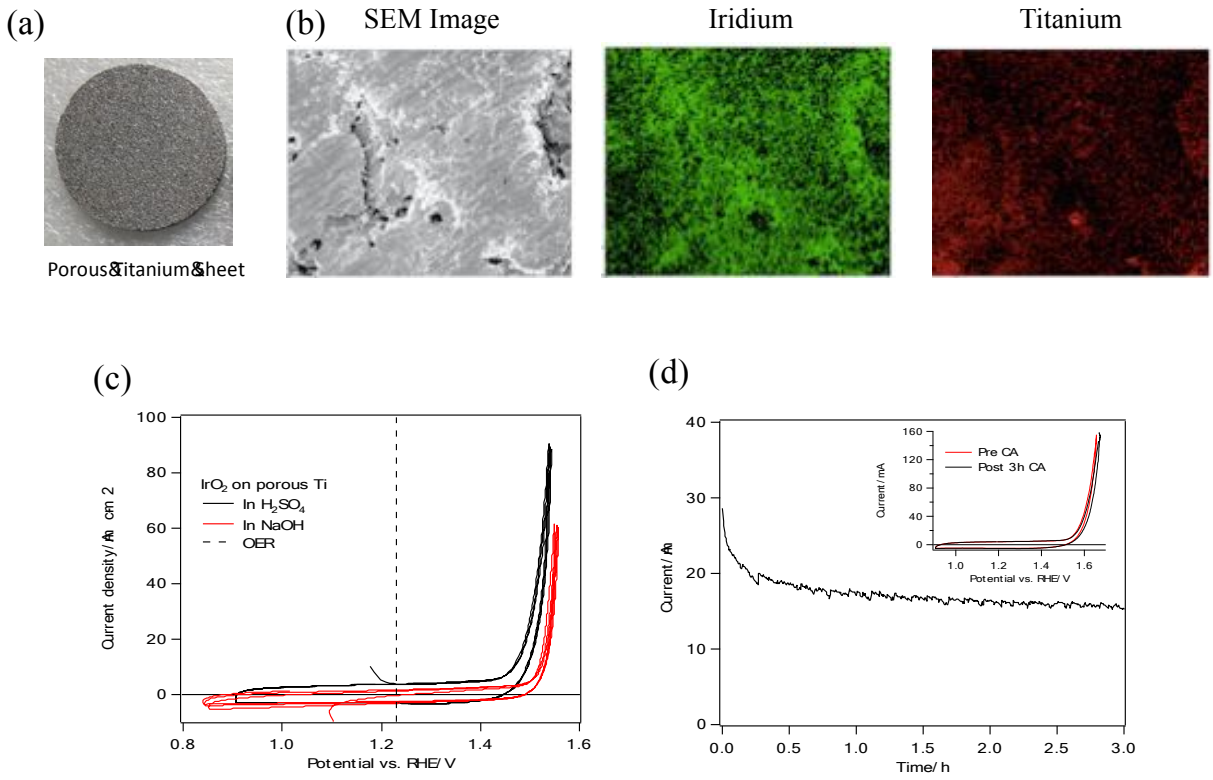

Fig. 4(a) – Image of porous Ti sheet used as substrate for OER catalyst deposition; (b) SEM image and Auger mapping of IrO_x deposited on porous Ti showing uniform coverage of Ir; (c) cyclic voltammetry measured with an IrO_x-coated porous Ti anode, with the dashed vertical line indicating the thermodynamic potential for the oxygen evolution reaction; (d) chronoamperometry showing current decay over 3 hours; inset: CV sweeps showing no performance degradation after 3 hours of chronoamperometry.

Figure 5

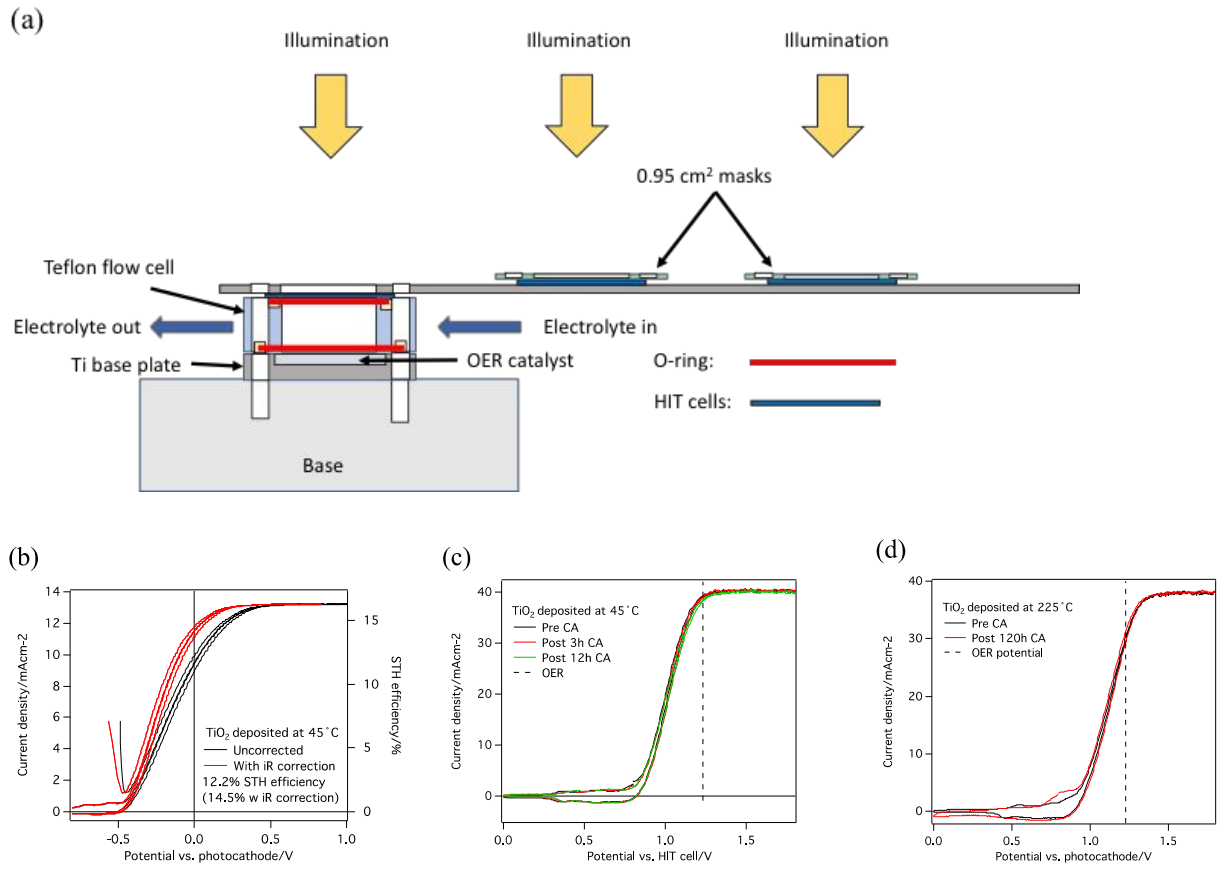

Fig. 5(a) – Schematic of the flow cell design used to perform unassisted water splitting; (b) J-V curve for triple cell device in a two-electrode configuration. The photocathode HIT cell is protected by TiO_2 deposited at 45°C. The current density at 0 V indicates a STH efficiency of 12.2% in 1 M H_2SO_4. With resistance correction, the STH efficiency is 14.5%; (c) cyclic voltammetry scans before and after each chronoamperometry testing; (d) cyclic voltammetry scans for a HIT cell with 35 nm of TiO_2 deposited at 225°C before and after 120 h of chronoamperometry testing.

Table 1

All efficiencies are measured under 1 sun illumination using a 2 electrode setup.

Absorber	Configuration	Efficiency	Stability	Reference
Tandem a-Si on p-Si	PEC-anode	3%	1 h	Sakai (1988)[20]
Triple junction a-Si	PEC-anode	7.80%	2 h	Rocheleau (1998)[22]
Triple junction a-Si	PEC-anode	7.80%	-	Khaselev (2001)[23]
Triple junction a-Si	PEC-cathode	4.70%	3 h	Reece (2011)[25]
4 c-Si cells in series	PV+E	10%	7 days	Cox (2014)[34]
Triple junction a-Si:H/a-Si:H/uc-Si:H	PEC-anode	9.5%	4 h	Urbain (2016)[26]
3 a-Si HIT cells	PV+E	14.20%	100 h	Schutaff (2016)[30]
4 a-SHJ/HIT cells	PV+E	9.50%	25 h	Song (2017)[29]
3 c-Si PV cells	PV+E	10.8%	48 h	Zhou (2018)[35]
4 c-Si PV cells	PV-PEC	9.8%	100 h	Fan (2019)[33]
3 a-Si HIT cells	PEC-anode	12.2%	> 120 h	This work

References

1. Gust, D., Moore, T. A. T. & Moore, A. L. AL. Solar fuels via artificial photosynthesis. *Acc. Chem. Res.* **42,** 1890–1898 (2009).
2. Fu, R. *et al.* U . S . Solar Photovoltaic System Cost Benchmark : Q1 2017 U . S . Solar Photovoltaic System Cost Benchmark : Q1 2017. (2017).
3. Gurudayal, G. *et al.* Efficient solar-driven electrochemical CO_2 reduction to hydrocarbons and oxygenates. *Energy Environ. Sci.* 2222–2230 (2017). doi:10.1039/C7EE01764B
4. Julian, K. & Holcroft, B. Economic and Business Perspectives. in *Photoelectrochemical Hydrogen Production* 277 (2012). doi:10.1007/978-1-4614-1380-6
5. Pinaud, B. A. *et al.* Technical and economic feasibility of centralized facilities for solar hydrogen production via photocatalysis and photoelectrochemistry. *Energy Environ. Sci.* **6,** 1983 (2013).
6. Newman, J., Hoertz, P. G., Bonino, C. A. & Trainham, J. A. Review: An Economic Perspective on Liquid Solar Fuels. *J. Electrochem. Soc.* **159,** A1722–A1729 (2012).
7. Trainham, J. A., Newman, J., Bonino, C. A., Hoertz, P. G. & Akunuri, N. Whither solar fuels? *Curr. Opin. Chem. Eng.* **1,** 204–210 (2012).
8. Carmo, M., Fritz, D. L., Mergel, J. & Stolten, D. A comprehensive review on PEM water electrolysis. *Int. J. Hydrogen Energy* **38,** 4901–4934 (2013).
9. Fujishima, A. & Honda, K. Electrochemical photolysis of water at a semiconductor electrode. *Nature* **238,** 37–38 (1972).
10. Hodes, G., Cahen, D. & Manassen, J. Tungsten trioxide as a photoanode for a photoelectrochemical cell (PEC). *Nature* **260,** 312–313 (1976).
11. Watanabe, T., Fujishima, A. & Honda, K. Photoelectrochemical Reactions at SrTiO3 Single Crystal Electrode. *Bulletin of the Chemical Society of Japan* **49,** 355–358 (1976).
12. Inoue, T. & Yamase, T. Photoelectrochemical cells using SiC for water splitting. *Chem. Lett.* 869–872 (1985).
13. Licht, S. *et al.* Efficient Solar Water Splitting, Exemplified by RuO2 -Catalyzed AlGaAs/Si Photoelectrolysis. *J. Phys. Chem. B* **104,** 8920–8924 (2000).
14. Khaselev, O. & Turner, J. A. A monolithic photovoltaic-photoelectrochemical device for hydrogen production via water splitting. *Science (80-.).* **280,** 425–427 (1998).
15. Jia, J. *et al.* Solar water splitting by photovoltaic-electrolysis with a solar-to-hydrogen efficiency over 30%. *Nat. Commun.* **7,** 1–6 (2016).
16. Nakamura, A. *et al.* A 24.4% solar to hydrogen energy conversion efficiency by combining concentrator photovoltaic modules and electrochemical cells. **107101,** 0–4 (1882).
17. Peharz, G., Dimroth, F. & Wittstadt, U. Solar hydrogen production by water splitting with a conversion efficiency of 18%. *Int. J. Hydrogen Energy* **32,** 3248–3252 (2007).
18. Shaner, M. R., Atwater, H. A., Lewis, N. S. & McFarland, E. W. A comparative technoeconomic analysis of renewable hydrogen production using solar energy. *Energy Environ. Sci.* **9,** 2354–2371 (2016).
19. Luo, J. *et al.* Water photolysis at 12.3% efficiency via perovskite photovoltaics and Earth-abundant catalysts. *Science (80-.).* **345,** 1593–1596 (2014).
20. Sakai, Y., Sugahara, S., Matsumura, M., Nakato, Y. & Tsubomura, H. Photoelectrochemical water splitting by tandem type and heterojunction amorphous

silicon electrodes. *Can. J. Chem.* **66,** 1853 (1988).
21. Lin, G. H., Kapur, M., Kainthla, R. C. & Bockris, J. O. M. One step method to produce hydrogen by a triple stack amorphous silicon solar cell. *Appl. Phys. Lett.* **55,** 386–387 (1989).
22. Rocheleau, R. E., Miller, E. L. & Misra, A. High-efficiency photoelectrochemical hydrogen production using multijunction amorphous silicon photoelectrodes. *Energy and Fuels* **12,** 3–10 (1998).
23. Khaselev, O., Bansal, A. & Turner, J. A. High-efficiency integrated multijunction photovoltaic/electrolysis systems for hydrogen production. *Int. J. Hydrogen Energy* **26,** 127–132 (2001).
24. Urbain, F. *et al.* Application and modeling of an integrated amorphous silicon tandem based device for solar water splitting. *Sol. Energy Mater. Sol. Cells* **140,** 275–280 (2015).
25. Reece, S. Y. *et al.* Wireless Solar Water Splitting Using Silicon-Based Semeiconductors and Earth-Abundant Catalysts. *Science (80-.).* **334,** 645–648 (2011).
26. Urbain, F. *et al.* Multijunction Si photocathodes with tunable photovoltages from 2.0 V to 2.8 V for light induced water splitting. *Energy Environ. Sci.* **9,** 145–154 (2016).
27. Masuko, K. *et al.* Achievement of more than 25% conversion efficiency with crystalline silicon heterojunction solar cell. *IEEE J. Photovoltaics* **4,** 1433–1435 (2014).
28. Wang, H. P. *et al.* High-performance a -Si/c-Si heterojunction photoelectrodes for photoelectrochemical oxygen and hydrogen evolution. *Nano Lett.* **15,** 2817–2824 (2015).
29. Song, H. *et al.* Bifunctional NiFe inverse opal electrocatalysts with heterojunction Si solar cells for 9.54%-efficient unassisted solar water splitting. *Nano Energy* **42,** 1–7 (2017).
30. Schüttauf, J.-W. *et al.* Solar-to-Hydrogen Production at 14.2% Efficiency with Silicon Photovoltaics and Earth-Abundant Electrocatalysts. *J. Electrochem. Soc.* **163,** F1177–F1181 (2016).
31. Döscher, H., Geisz, J. F., Deutsch, T. G. & Turner, J. A. Sunlight absorption in water – efficiency and design implications for photoelectrochemical devices. *Energy Environ. Sci.* **7,** 2951–2956 (2014).
32. Bae, D., Seger, B., Vesborg, P. C. K., Hansen, O. & Chorkendorff, I. Strategies for stable water splitting via protected photoelectrodes. *Chem. Soc. Rev.* **46,** 1933–1954 (2017).
33. Fan, R. *et al.* Unassisted solar water splitting with 9.8% efficiency and over 100 h stability based on Si solar cells and photoelectrodes catalyzed by bifunctional Ni–Mo/Ni. *J. Mater. Chem. A* (2019). doi:2018/TA/C8TA10165E
34. Cox, C. R., Lee, J. Z., Nocera, D. G. & Buonassisi, T. Ten-percent solar-to-fuel conversion with nonprecious materials. *Proc. Natl. Acad. Sci.* **111,** 14057–14061 (2014).
35. Zhou, X. *et al.* A bifunctional and stable Ni-Co-S/Ni-Co-P bistratal electrocatalyst for 10.8%-efficient overall solar water splitting. *J. Mater. Chem. A* **6,** 20297–20303 (2018).
36. Smith, R. D. L., Sporinova, B., Fagan, R. D., Trudel, S. & Berlinguette, C. P. Facile photochemical preparation of amorphous iridium oxide films for water oxidation catalysis. *Chem. Mater.* **26,** 1654–1659 (2014).
37. Nassreddine, S., Bergeret, G., Jouguet, B., Geantet, C. & Piccolo, L. Operando study of iridium acetylacetonate decomposition on amorphous silica–alumina for bifunctional catalyst preparation. *Phys. Chem. Chem. Phys.* **12,** 7812 (2010).
38. Chen, Y. W. *et al.* Atomic layer-deposited tunnel oxide stabilizes silicon photoanodes for water oxidation. *Nat. Mater.* **10,** 539–544 (2011).
39. Sunpreme. Symmetric Bifacial Architecture. Available at:

http://sunpreme.com/symmetric-bifacial-architecture/.
40. Ji, L. *et al.* A silicon-based photocathode for water reduction with an epitaxial SrTiO3protection layer and a nanostructured catalyst. *Nat. Nanotechnol.* **10,** 84–90 (2015).
41. Lin, Y. J. *et al.* Amorphous Si Thin Film Based Photocathodes with High Photovoltage for Efficient Hydrogen Production. *Nano Lett.* **13,** 5615–5618 (2013).
42. Klett, J. *et al.* Band engineering for efficient catalyst-substrate coupling for photoelectrochemical water splitting. *Phys. Chem. Chem. Phys.* **18,** 10751–10757 (2016).
43. Seif, J. P., Krishnamani, G., Demaurex, B., Ballif, C. & De Wolf, S. Amorphous/Crystalline Silicon Interface Passivation: Ambient-Temperature Dependence and Implications for Solar Cell Performance. *IEEE J. Photovoltaics* **5,** 718–724 (2015).
44. Zhang, D., Tavakoliyaraki, A., Wu, Y., Van Swaaij, R. A. C. M. M. & Zeman, M. Influence of ITO deposition and post annealing on HIT solar cell structures. *Energy Procedia* **8,** 207–213 (2011).
45. Xie, Q. *et al.* Atomic layer deposition of TiO2 from tetrakis-dimethyl-amido titanium or Ti isopropoxide precursors and H2O. *J. Appl. Phys.* **102,** 083521 (2007).
46. Kleider, J. P., Gudovskikh, A. S. & Roca I Cabarrocas, P. Determination of the conduction band offset between hydrogenated amorphous silicon and crystalline silicon from surface inversion layer conductance measurements. *Appl. Phys. Lett.* **92,** (2008).
47. McCrory, C. C. L. *et al.* Benchmarking Hydrogen Evolving Reaction and Oxygen Evolving Reaction Electrocatalysts for Solar Water Splitting Devices. *J. Am. Chem. Soc.* **137,** 4347–4357 (2015).
48. Gottesfeld, S. & Srinivasan, S. Electrochemical and optical studies of thick oxide layers on iridium and their electrocatalytic activities for the oxygen evolution reaction. *J. Electroanal. Chem.* **86,** 89–104 (1978).
49. Cherevko, S., Geiger, S., Kasian, O., Mingers, A. & Mayrhofer, K. J. J. Oxygen evolution activity and stability of iridium in acidic media. Part 2. - Electrochemically grown hydrous iridium oxide. *J. Electroanal. Chem.* **774,** 102–110 (2016).
50. Nakagawa, T., Beasley, C. A. & Murray, R. W. Efficient Electro-Oxidation of Water near Its Reversible Potential by a Mesoporous IrOx Nanoparticle Film. *J. Phys. Chem. C Lett.* 12958–12961 (2009).
51. Rausch, B., Symes, M. D., Chisholm, G. & Cronin, L. Decoupled catalytic hydrogen evolution from a molecular metal oxide redox mediator in water splitting. **345,** 2–7 (2014).
52. United States Department of Energy. Hydrogen Production. *Fuel Cell Technol. Off. Multi-Year Res. Dev. Demonstr. Plant* **11007,** 1–44 (2015).
53. Sathre, R. *et al.* Life-cycle net energy assessment of large-scale hydrogen production via photoelectrochemical water splitting. *Energy Environ. Sci.* **7,** 3264–3278 (2014).
54. Maruyama, E. *et al.* Sanyo's challenges to the development of high-efficiency HIT solar cells and the expansion of HIT business. *Conf. Rec. 2006 IEEE 4th World Conf. Photovolt. Energy Conversion, WCPEC-4* **2,** 1455–1460 (2007).
55. Heng, J. B. *et al.* >23% High-efficiency tunnel oxide junction bifacial solar cell with electroplated Cu gridlines. *IEEE J. Photovoltaics* **5,** 82–86 (2015).
56. Lim, G. T. & Kim, D. H. Characteristics of TiOx films prepared by chemical vapor deposition using tetrakis-dimethyl-amido-titanium and water. *Thin Solid Films* **498,** 254–258 (2006).

57. Correa, G. C., Bao, B. & Strandwitz, N. C. Chemical Stability of Titania and Alumina Thin Films Formed by Atomic Layer Deposition. *ACS Appl. Mater. Interfaces* **7,** 14816–14821 (2015).
58. King, L. A., Hellstern, T. R., Park, J., Sinclair, R. & Jaramillo, T. F. Highly Stable Molybdenum Disulfide Protected Silicon Photocathodes for Photoelectrochemical Water Splitting. *ACS Appl. Mater. Interfaces* **9,** 36792–36798 (2017).
59. Gong, M. *et al.* An advanced Ni-Fe layered double hydroxide electrocatalyst for water oxidation. *J. Am. Chem. Soc.* **135,** 8452–8455 (2013).
60. Lu, X. & Zhao, C. Electrodeposition of hierarchically structured three-dimensional nickel-iron electrodes for efficient oxygen evolution at high current densities. *Nat. Commun.* **6,** 1–7 (2015).
61. Kiejna, A. Work Function of Metals. *Ref. Modul. Chem. Mol. Sci. Chem. Eng.* (2014). doi:10.1016/B978-0-12-409547-2.11420-9
62. Park, Y., Choong, V., Gao, Y., Hsieh, B. R. & Tang, C. W. Work function of indium tin oxide transparent conductor measured by photoelectron spectroscopy. *Appl. Phys. Lett.* **68,** 2699–2701 (1996).